

# Aggregation of bead-monolayers in flat microfluidic chambers – simulation by the model of porous media

Markus Grumann,<sup>a</sup> Michael Dobmeier,<sup>a</sup> Patric Schippers,<sup>a</sup> Thilo Brenner,<sup>a</sup> Claus Kuhn,<sup>b</sup> Michael Fritsche,<sup>b</sup> Roland Zengerle<sup>a</sup> and Jens Ducreé<sup>a</sup>

<sup>a</sup> IMTEK – Institute of Microsystem Technology, Lab for MEMS Applications, University of Freiburg, Georges-Koehler-Allee 103, D-79110 Freiburg, Germany

<sup>b</sup> Fraunhofer Institute Manufacturing Engineering and Automation (FhG-IPA), D-70569 Stuttgart, Germany

www.rsc.org/loc



Received 24th October 2003, Accepted 16th December 2003  
First published as an Advance Article on the web 9th February 2004

In this paper, we for the first time simulate the process of hydrodynamic bead aggregation in a flat micro-fluidic chamber by a porous-media model in an iterative routine. This allows us to optimize the chamber design of our recently developed experimental method to form periodical monolayers from the flow of bead suspension. Periodical monolayers are advantageous for parallel assay formats since they enhance the mechanical rigidity of the aggregated pattern. This is important to avoid a spatial rearrangement along various steps of a read-out procedure which would impair the correlation between measurements. Furthermore, the monolayer formation guarantees the individual optical accessibility of all probe beads. By modelling the monolayers with porous media, we can drastically reduce the degrees of freedom in a two-phase, multi-particle problem. This way, we are able to compute stationary hydrodynamic flow patterns in the chamber. In order to simulate the complete filling process from these stationary solutions, we developed an iterative master routine which takes the transient aggregation pattern as the initial condition, then evaluates the placement of the newly introduced beads, and finally converts the points of aggregation into porous media.

## Introduction

Microfluidic technologies are increasingly used to miniaturize analytical instruments to form so-called “lab-on-a-chip” devices.<sup>1,2,3,4</sup> Striking advantages of these lab-on-a-chip concepts are the small volume of sample and reagents as well as the increased process integration and automation on behalf of the technological backend. For the consumer, this means an enhanced ease of use, faster time-to-results, and, eventually, appreciable cost savings. Various lab-on-a-chip concepts have been described and the first commercial products have been launched.<sup>5,6,7,8</sup>

Bead-based assays are a well established analytical method for multi parameter screening of a given sample. Beads are spherical particles made of polymers or glass with diameters of between a few and several hundred micrometers. They are commercially available in a huge variety of materials and coatings<sup>10</sup> from different suppliers.<sup>11,12,13</sup> Beads add functionality to microfluidic devices which is difficult to achieve otherwise.<sup>14</sup> They can be used as passive components (e.g. as the solid phase in chemical reactions)<sup>15,16</sup> or as active components (e.g. as a stirrer for mixing of fluids or as an actuator for liquid pumping).

In a bead-based assay, an ensemble of beads is exposed to a liquid sample. Prior to the assay, each bead is coated with a designated biosensitive layer to detect a specific target molecule in the sample. Compared to other parallel assays such as microarrays,<sup>17</sup> bead-based analytical methods are favorable in terms of ease of preparation, enhanced reaction kinetics, and reduction of “dead surface” on the solid substrate which normally have to be blocked to avoid unspecific binding.

However, a major task to be solved is the implementation of readout as each bead has to be localized and identified in an *a priori* unsorted spatial distribution. One common method to identify the beads are dyes. The effective bandwidth which is broadened by stray light and shadow usually limits the degree of parallelism. To localize the beads, the suspension is usually aligned in a file by means of a tiny channel. In a setup resembling a conventional flow-cytometer, a sequential readout is realized *via* a downstream

detector. In a microfluidic platform, a modular setup often consists of a disposable microchip and a separate detection system.<sup>9</sup>

The primary goal of this work is to optimize the formation of periodical monolayers in a flat microfluidic chamber from the flow of bead suspensions. The periodicity allows a facilitated and automated readout similar to the Cartesian alignment of spots in a microarray.<sup>18</sup> In addition, the stability of the formation allows the sequential flow of several reagents over the beads without changing their conformation. Our experimental investigations showed that the key parameters determining the periodicity, reproducibility, and mechanical stability are the geometry of the microfluidic guide structures and the applied pressure.<sup>19</sup> A rhombus-like aggregation chamber with an aperture angle of 60° and a single outlet channel proved to create the most stable aggregation pattern in a hexagonal monolayer lattice. This form of the chamber is also advantageous for rinsing during washing processes as it is required for immunoassays. The filling ratios of rhombus-shaped chambers are almost independent of the inlet pressure, which enables filling of the chip at comparably low and loosely controlled pressures to simplify experimental setups.

The complex problem of simulating the flow of multiparticle suspensions is the subject of research with different approaches.<sup>22,23,24</sup> In this paper, the hydrodynamic interaction of liquid flow with a stationary monolayer of beads is modelled by the flow through porous media. Porous media are common in hydrology and related fields, where the behavior of fluidic transport has to be described in a macroscopic approach.<sup>25</sup> Hydrodynamic penetration of liquid is described by the Navier–Stokes Equation, the Stokes law of friction (two-phase flow simulation) and Darcy’s law of flow through porous media. Darcy’s law provides a linear relationship between the filter velocity of a liquid through a porous medium and the pressure gradient at laminar conditions. We have implemented this model by the commercial code FIDAP (release 8.7.0 of Fluent Inc.) which is called in an iterative fashion for each stage of filling by a master script.<sup>20,21</sup>

The paper is structured as follows. In the first section, the experimental setup and results of the aggregation of beads are

discussed. Next, the simulation of this process is presented at the initial phase of filling and with a partially-filled aggregation chamber. After this the model of porous media is introduced and evaluated to describe the complete process of filling before a final summary and conclusion.

## Aggregation of bead-monolayers in microfluidic chambers

We have recently proposed a concept to carry out immunochemical reactions and detection inside a flat chamber where the beads can aggregate in the form of a monolayer.<sup>19</sup> In our investigations, the beads act as a solid phase for immobilized biochemical probes. They are used to fill the detection chamber prior to processing a diagnostic assay.

All experiments were carried out with PMMA beads possessing a mass density of  $1190 \text{ kg m}^{-3}$  and a diameter of  $180 \text{ }\mu\text{m}$ .<sup>11</sup> The aggregation chips feature a central bead-chamber measuring  $6 \times 6 \times 0.19 \text{ mm}^3$  (Fig. 1). With  $200 \text{ }\mu\text{m}$ , the chamber depth is always kept only slightly higher than the diameter of the beads in order to enforce the alignment in a monolayer.<sup>9</sup> In front of the outlets possessing a depth of  $100 \text{ }\mu\text{m}$ , only, the beads thus accumulate and successively fill the chamber.

The microfluidic aggregation chip is made of two PMMA plates with dimensions of  $40 \times 30 \times 10 \text{ mm}^3$ . The bottom chip always hosts the structures while the upper chip is merely a cover held by four fixing screws. All microfluidic structures have been fabricated by CNC machining with a typical minimum structure size of  $100 \text{ }\mu\text{m}$ .

In our setup, the completely filled aggregation chamber features far more than 1000 beads, allowing it to carry out highly parallel assays. This multitude of beads may be readily functionalized by a conventional off-disk procedure – in several batches. Each batch represents beads which are coated with one specific protein probe. After filling a designated mixture of beads into the microfluidic device, the statistical distribution of the mixed beads throughout the flat chamber requires a consistent spatial mapping between different analytical steps. This is best realized when the beads rest at fixed spatial positions during the entire assay. In our method, the required mechanical stability is established by packing the beads as tight as possible in a regular lattice, *i.e.* in a 2-dimensional, hexagonal structure.

Another benefit of the aggregation in a monolayer is that all beads directly face the detection unit, ruling out optical occlusion as in 3-dimensional aggregation patterns. Thus, in addition to the fixed spatial mapping, the formation of monolayers enables individual optical addressing and read-out.

## Simulation of bead-aggregation

To our knowledge, no commercial CFD tool is currently available which is capable of simulating the hydrodynamic flow of a suspension containing numerous spatially expanded particles, taking into account all types of interaction between particles, the

walls and the liquid matrix.<sup>28</sup> A model based on coupled two-phase flow incorporating porous media is the most feasible. Evaluating FIDAP, release 8.7.0 of Fluent Inc. as the most appropriate simulation tool, we visualized and analyzed the process of bead aggregation. All simulations were carried out using the above-mentioned chamber geometry (Fig. 1). The geometry and the inserted mesh was designed with Gambit (Rel. 2.4.0). Generally, the simulations remain numerically stable up to an inlet pressure of typically  $30 \text{ kPa}$ . Exceeding this boundary leads to non-reliable results.

## Initial phase of filling

In the initial phase of filling, the main parameters affecting the flow pattern inside the bead chamber are the ratio of the hydrodynamic resistances of the outlet channels. This resistance ratio scales with the ratio of the flow-rates of the outlet channels in a reciprocal fashion. To further check consistency with a simulation of a homogenous fluid, we also verified that the total flow passing the cross-sectional area of each outlet channel with a given length linearly depends on the inlet pressure as predicted by the law of Hagen–Poiseuille.

## Particle interactions with liquid

To carry out a simulation of the bead suspension, the coupling between beads and fluid has to be analyzed. For a numerical simulation, we drastically have to reduce the complexity of the system by appropriate simplifications. The particles are thus implemented in FIDAP as point-like bodies to eliminate the complex boundary conditions of the bead surface. This way, the aggregation due to the geometrical barrier cannot be directly observed and bead–bead interactions are discarded at this stage (Fig. 2). Later in this paper, the interaction between incoming beads and the static pattern of aggregated beads is introduced again. However, the mutual interaction between fluid and particles is still taken into account according to Stokes' law.

In suspension, the beads are simulated as mass points possessing a mass of  $3.6 \text{ }\mu\text{g}$  and  $7.6 \text{ }\mu\text{g}$  which corresponds to our  $180 \text{ }\mu\text{m}$  beads made of PMMA and borosilicate, respectively. Only for the viscous (Stokes) drag, the spatial extension of the beads is taken into account. To simulate the movement of 40 beads in the carrier fluid in Fig. 2, particles (*e.g.*, beads) are generated at 40 positions which are linearly distributed throughout the entrance area of the common inlet. The simulated movement of the suspended particles is analyzed using particle path plots. The particle count of the outlet channels is determined by individually tracking the trajectories of the beads into the outlet channels. The interaction between entering and previously aggregated between is not considered at this first stage.

Similar to the ratio of flow-rates at the two outlets, the ratio of the particle counts  $I_1/I_2$  of the outlet channels depends reciprocally on the ratio of the hydrodynamic resistances. Or, *vice versa*, the inverse ratio of particle counts  $I_2/I_1$  depends linearly on the ratio of

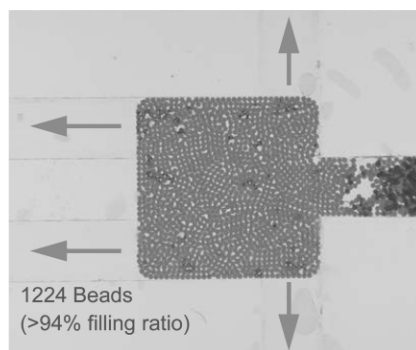
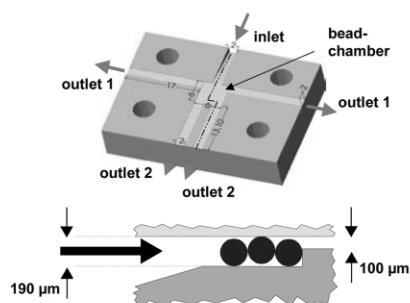


**Fig. 1** Schematic drawing of the microfluidic chip (left) and the depth profile following the dot-dashed line in the 3D view. Completely filled chamber with beads made of PMMA at a diameter of  $180 \text{ }\mu\text{m}$  and mass density of  $1190 \text{ kg m}^{-3}$  (right).

hydrodynamic resistances. In contrast to the flow pattern of the fluid, the beads increasingly prefer outlet channel 2 as the mass density of the beads grows. Therefore, the higher the specific density of the beads the more the trajectories deviate related to the fluid. This can be explained by the inertia of the beads.

### The model of the porous media

Theoretically, accumulated beads at a geometrical constraint create a hydrodynamic resistance which must be passed by the subsequent fluid. Thus, aggregated beads reduce the remaining free volume of the aggregation chamber and locally elevate the hydrodynamic resistance of the outlet geometry. In the region of a porous media the Navier–Stokes equation is extended to

$$\rho \left[ \frac{1}{\phi} \frac{\partial \vec{v}}{\partial t} + \frac{1}{\phi^2} (\vec{v} \nabla) \vec{v} \right] = -\nabla_p + \eta_e \nabla^2 \vec{v} + \rho \vec{g} - \left( \frac{\eta}{[K]} \vec{v} + a \rho |\vec{v}| \vec{v} \right) \quad (1)$$

whereas the additional parameters porosity  $\phi$ , effective viscosity  $\eta_e$ , Forchheimer-coefficient  $a$ , and permeability  $[K]$  have to be taken into account.

The porosity is defined as

$$\phi = \frac{V_f}{V_{ges}} \quad (2)$$

and describes the fraction of the free remaining volume with respect to the total volume.

In 1856 Henry Darcy adapted for porous media the linear relationship between a driving pressure gradient and the resulting fluid velocity  $\vec{v}$  with the permeability  $[K]$ .

$$F = -\nabla_p = \frac{\eta}{[K]} \vec{v} \quad (3)$$

In case of anisotropic media, the permeability  $[K]$  exhibits a 3 × 3 matrix structure. Though the equation of Darcy is only valid in the

laminar regime, in 1901 Philipp Forchheimer expanded the equation of Darcy with  $(\rho v^2)$  in order to explain the non-linear behavior of porous media in the turbulent regime.

$$-\vec{F} = -\nabla_p = \frac{\eta}{[K]} \vec{v} + a \rho |\vec{v}| \vec{v} \quad (4)$$

The Forchheimer-coefficient  $a$  is experimentally determined for different types of porous media.<sup>29</sup> An analytical description of  $a$  and  $[K]$  was given by S. Ergun in 1952 with

$$a = \frac{1.75}{\sqrt{150\phi^3}} \quad (5)$$

and

$$K = \frac{\phi^3 d_p^2}{150(1-\phi)^2} \quad (6)$$

For a periodical monolayer of beads with a diameter of 180  $\mu\text{m}$  and quadratic aggregation pattern the porosity and the permeability are set to  $a = 0.476$  and  $K = 8.5 \times 10^{-11} \text{m}^2$ .

### Evaluation of the porous media concept

To run CFD-simulations with porous media, FIDAP offers a model (POROUS ENTITY) where the Navier–Stokes Equation is extended with the equations of Darcy, Forchheimer and Ergun. However, to model monolayers of beads as porous media, we first had to evaluate the equivalent porosity of a locally aggregated monolayer of beads. To this end, a symmetric channel structure comprising one inlet and two outlet channels was designed and fabricated in PMMA (Fig. 3, right plot). The outlet channels are confined by a geometrical barrier, thus forcing the beads to accumulate and create a monolayer. Both experimental investigations and simulations were carried out: In the experiment, the beads were placed manually into one of the outlet channels. The

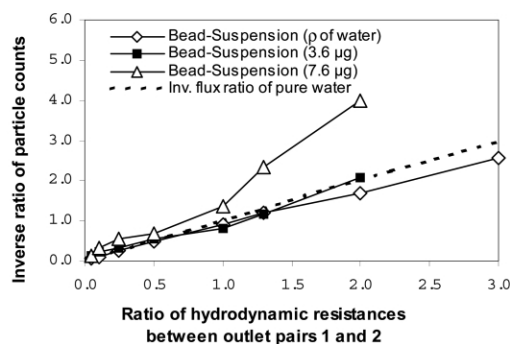
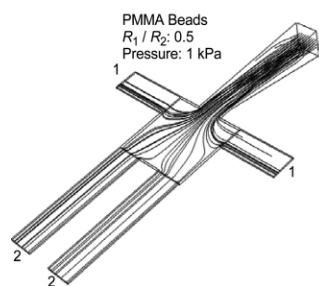


**Fig. 2** Left: simulation of the particle path plots of 40 beads (3.6  $\mu\text{g}$ ) for an inlet pressure of 1 kPa and a ratio  $R_1/R_2 = 0.5$  of the hydrodynamic resistances of the upper and lower outlet pairs  $R_1$  and  $R_2$ , respectively. Right: flow characteristics of bead-suspensions at varying ratios of hydrodynamic resistance for an inlet pressure of 1 kPa. The particle count  $I_x$ ,  $x = \{1, 2\}$  of the outlet channel  $x$  is given by counting the number of trajectories of the beads at the end of outlet  $x$ . A ratio of the hydrodynamic resistances of  $R_1/R_2 = 1.29$  leads to an inverse ratio of particle counts of  $I_2/I_1 = 1.16$  for beads with a mass of 3.6  $\mu\text{g}$ . The interaction between incoming beads and aggregated beads is discarded.

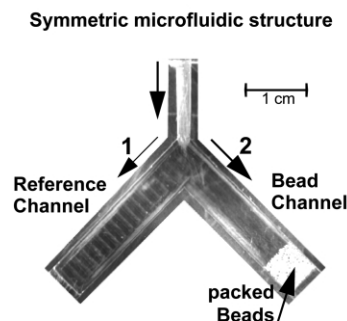
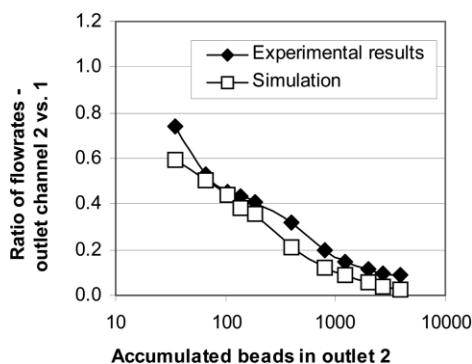


**Fig. 3** Impact of accumulated beads to the flow-rate: comparison of experimental results with simulations. The effective viscosity and the internal FIDAP parameter as fitting parameters with  $\eta_e = 10^{-1} \text{Pa s}$  and  $A = 10^{-2}$ , respectively, were found to fit most suitably (left plot). The symmetrical microfluidic structure was designed and both fabricated by CNC-machining and implemented in FIDAP. Beads were accumulated in outlet channel 2 in front of the geometrical barrier (right plot).

corresponding area covered by the beads were filled with porous media in the simulation.

A series of experiments were performed involving different numbers of aggregated beads in the right-hand channel, ranging between 0 to nearly 4000, to record the ratio of the flow-rates. With a growing degree of aggregation, the hydrodynamic resistance of the right outlet channel becomes far greater than the unoccupied left channel resulting in a decreasing ratio of flow-rates between the right and the left channel, respectively. Each experimentally detected ratio of flow-rate was subsequently approached by a set of simulations with varying fit-parameters effective viscosity  $\eta_e$  and the internal FIDAP A-coefficient. Here, FIDAP proposes to adjust  $\eta_e$  and A in a way that  $A = \eta/\eta_e$  and  $\eta$  as the viscosity of the carrier-fluid. Since the monolayer of aggregated beads had to be adapted in the model of porous media, first a parameter study was carried out.

A fit to the experimental results leads to the determination of the free parameters for the simulation (Fig. 3). An extensive numerical fit determined the internal FIDAP A-coefficient ( $A = 10^{-2}$ ) and the effective viscosity of the accumulated beads ( $\eta_e = 0.1 \text{ Pa s}$ ) – which turns out to be roughly 100-fold higher than pure water.

### Automated iterative simulation of the filling process

To investigate the complete filling of the aggregation chamber, the hydrodynamic resistance of the contribution of the already accumulated beads has to be taken into account. An iterative JAVA routine has been developed, placing at each step the newly aggregated bead according to the calculated particle trajectories. The simulation of the iterative “bead-by-bead” filling process would be closest to the physical conditions, though this is not practicable due to its excessive computation time. Hence, the width of the steps was typically set to 10 beads per iteration. The numerical mesh size of the aggregation chamber was set to  $(200 \mu\text{m})^3$  which adapted to the bead diameter of  $180 \mu\text{m}$  leads to 900 cubicles for the entire aggregation chamber.

At the beginning of each iterative step, a spatial distribution of the porous media inside the aggregation chamber is taken from the preceding step to define new hydrodynamic boundary conditions (Fig. 4, “start”). Next, the set of particles is launched and the

resulting trajectories are analyzed to pinpoint so-called “cells of observation” (Fig. 4a). These are cells which are connected to the outlet or whose adjacent cells were previously switched to porous media. In other words, a cell of observation marks a potential position for the subsequent aggregation of a bead. In the next step, the geometrical coordinates of all bead trajectories are scanned for a point of intersection with one of the observed cells (Fig. 4b). In case several candidates for a possible attachment are evaluated along the same trajectory, the cell of observation is chosen which represents the outermost point of the particle trajectory that is still inside the aggregation chamber. At the end of the multi-particle iteration step, all selected cells are turned into porous media (Fig. 4c).

Applying the master routine to the microfluidic design shown in Fig. 1, we found good coincidence of experimental and simulation results (Figs. 5 and 6). During the initial phase of filling, the flow properties of the bead suspension are determined by the distribution of the (undisturbed) hydrodynamic resistances of the four outlets and the previous results (Fig. 2) are applicable. In this phase, separate clusters of aggregated beads emerge, their location and also the shape is in good qualitative agreement with the experimental observation. At the beginning, the ratio of particle aggregation in front of the upper and lower outlet channels 1 and 2 is found to be  $I_1/I_2 = 0.53$ . Along the filling process, Fig. 6 reveals that the flow distribution dynamically adjusts to a transient aggregation pattern in a way that the rates of aggregation at the two types of outlets seek to match (*i.e.*,  $I_1/I_2 \rightarrow 1$ ).

### Conclusion

Experimental and simulative investigations were carried out to demonstrate that the hydrodynamic properties of locally aggregated monolayers of beads can be modelled by porous media. The equivalent hydrodynamic resistance of aggregated beads was determined experimentally by flow rate measurements and compared to simulations of the flow through porous media.

The two phase flow simulation was used to investigate the flow properties of the beads in an aggregation chamber and to calculate their particle trajectories. The simulation results were successfully verified by experimental measurements. Initially, the spatial distribution of the aggregated beads is governed by the geometrical shape of the aggregation chamber and the local distribution of the

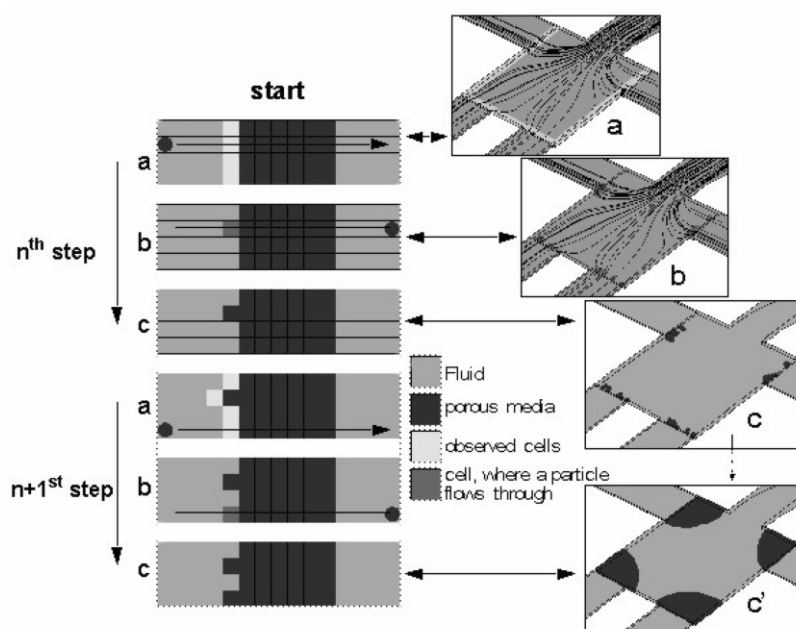


**Fig. 4** Concept of the master routine which analyzes the rest positions of the particles in each simulation step and, accordingly, activates porous cells as static boundary condition for the consecutive step. (a) For a given configuration of porous cells (dark gray), the cells of observation (bright gray) are identified and activated. (b) The point of intersection between the particle trajectory and the layer of observed cells are identified. (c) This cell is switched to porous media (dark gray).

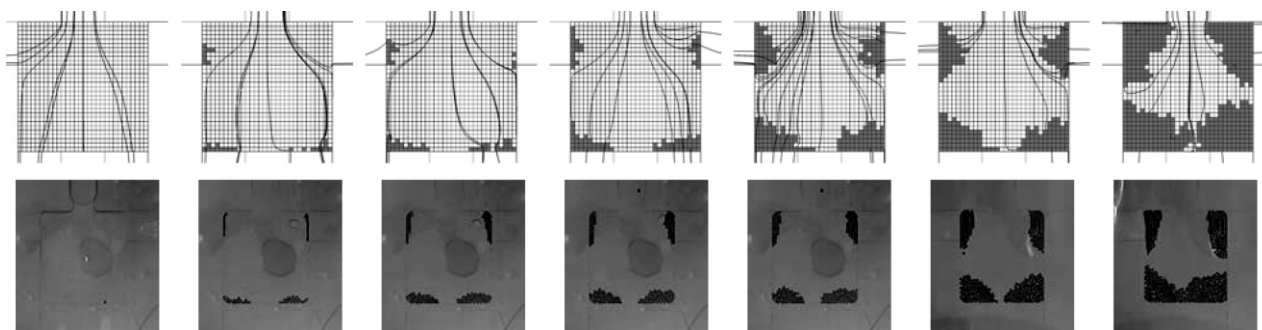


**Fig. 5** Complete course of filling. Iterative two-phase-flow-simulation (upper sequence). Video-frame sequence at an inlet pressure of 20 kPa (lower sequence). Initially, four separate zones of aggregated beads emerge during filling. The spatial distribution of the aggregated beads is governed by the geometry of the aggregation chamber and the pattern of the previously aggregated beads, *i.e.* the porous zones in our modelling.

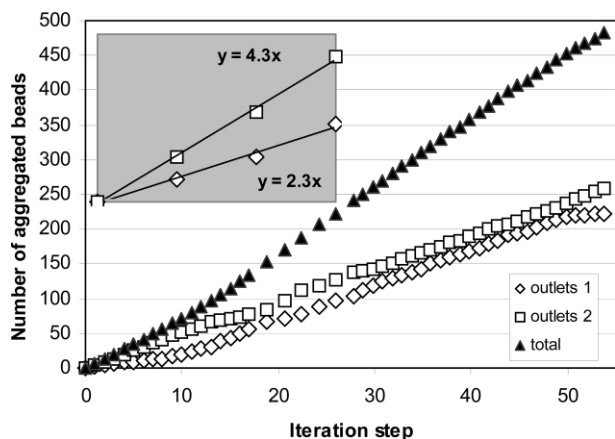


**Fig. 6** Iterative simulation of the complete process of filling. At the initial phase of filling (until iteration step 4, see inset) the number of aggregated beads in front of outlet 1 and outlet 2 respectively follows a ratio of  $2.3/4.3 = 0.53$ . The redistribution of flow pattern caused by the modification of the distribution of the hydrodynamic resistance equalizes this completely for the ongoing filling process.

hydrodynamic resistance. We found that during the process of filling, the distribution of aggregated beads seeks to balance the flow rates through the upper and lower outlet channels.

Our model can be extended to all problems involving the complex interaction between beads which are suspended in the flow and assemblies of beads which have aggregated at high particle densities at fixed positions in a microfluidic chamber. The iterative routine furthermore allows visualization of the full course of a dynamic aggregation process.

## References

- 1 K. Sato, M. Yamanaka, H. Takahashi, K. Uchiyama, M. Tokeshi, H. Katou, H. Kimura and T. Kitamori, Integrated Immunoassay System using Multichannel Microchip for Simultaneous Determination, *Proceedings of  $\mu$ TAS Conference*, ed. J. Ramsey and A. van den Berg, 2001, pp. 511–512.
- 2 M. Madou, L. Lee, S. Daunert, S. Lai and C. Shih, Design and Fabrication of CD-like microfluidic Platforms for Diagnostics: Microfluidic Functions, *Biochemical Microdevices*, 2001, vol. 3:3, pp. 245–254.
- 3 J. Ducrée, T. Brenner, M. Grumann, W. Bessler, M. Stelzle, S. Messner, T. Nann, J. Ruehe, I. Moser and R. Zengerle, *Bio-Disk – A centrifugal platform for integrated point-of-care diagnostics on whole blood*, www.bio-disk.com.
- 4 J. Ducrée, T. Brenner, T. Glatzel and R. Zengerle, A Coriolis-Based Split-and-Recombine Laminator for Ultrafast Mixing on Rotating Disks, *Proceedings of  $\mu$ Tas Conference*, ed. M. Northrup, K. Jensen and D. Harrison, 2003, pp. 603–606.
- 5 Gyros AB, Sweden, www.gyros.com.
- 6 Flowmap – microfluidics roadmap for the life-sciences, www.microfluidics-roadmap.com.
- 7 Tecan Group Ltd, Switzerland, www.tecan.com.
- 8 Caliper Technologies Corp., USA, www.calipertech.com.
- 9 C. Kuhn, M. Fritsche, T. Brenner, M. Grumann, M. Dobmeier, P. Schippers, R. Zengerle, J. Ducrée, C. Stähler, P. Stähler and F. Stähler, Fluidic Microchip for bead based Assay Systems, *Bioforum International*, 02/2003.
- 10 B. Sinclair, To Bead or not to Bead: Applications of Magnetic Bead Technology, *The Scientist*, June 22, 1998, 12, (13), 17.
- 11 Micro particles GmbH, Germany, www.microparticles.de.
- 12 Bangs Laboratories Inc., USA, www.bangslabs.com.
- 13 Dynal Biotech, Norway, www.dynabead.com.
- 14 P. Griss, H. Andersson, W. v. der Wijngaart and G. Stemme, Beads in Biochemical Microfluidics, *Proceedings of  $\mu$ TAS Conference*, ed. Y. Baba, S. Shoji and A. van den Berg, 2002, vol. 2, pp. 605–607.
- 15 K. Sato, M. Tokeshi, T. Otake, H. Kimura, T. Ooi, M. Nakao and T. Kitamori, Integration of Immunosorbent Assay Systems into a Multi-channel Microchip for clinical Diagnoses, *Proceedings of  $\mu$ TAS Conference*, ed. W. Olthuis, P. Bergveld and A. van den Berg, 2000, pp. 513–515.
- 16 G. Lettieri, E. Verpoorte and N. de Rooij, Affinity-based Bioanalysis using freely moving Beads as Matrices for heterogeneous Assays, *Proceedings of  $\mu$ TAS Conference*, ed. J. Ramsey and A. van den Berg, 2001, pp. 503–504.
- 17 *Nature Genetics Supplement*, January, 1999, vol. 21, no. 1.
- 18 J. Ducrée, H. Gruhler, N. Hey, M. Mueller, S. Bekesi, M. Freygang, H. Sandmaier and R. Zengerle, TOPSPOT – a new Method for the Fabrication of Microarrays, *Proceedings of MEMS conference*, 2000, pp. 317–322.
- 19 M. Grumann, P. Schippers, M. Dobmeier, S. Haerberle, A. Geipel, T. Brenner, C. Kuhn, M. Fritsche, R. Zengerle and J. Ducrée, Formation of hexagonal Monolayers by Flow of Bead Suspensions into flat Microchambers, *Proceedings of IMECE Conference 2003 of ASME*, 2003, 41427.
- 20 A. Sharp, Shear-Induced Arching of Particle-Laden Flows in Microtubes, *Proceedings of IMECE conference of ASME 2001*, 2001, 23879.
- 21 B. Stoeber, E. Espanol and D. Liepmann, Operational Limits of Suspension Flows through Sudden Concentrations, *Proceedings of IMECE Conference, ASME*, 2001.
- 22 B. Pandian, K. Shah, S. Sundaram and V. Makhinjani, Biochemical Binding in Microsphere-based Assays, *Proceedings of MSM Conference*, 2002, pp. 92–95.
- 23 R. Maier, D. Kroll, Y. Kutsovsky, H. Davis and R. Bernadet, Simulation of flow through bead packs using the lattice Boltzmann method, *Phys. Fluids*, 1998, 10(1), 60–74.
- 24 J. Berthier, P. Pham and P. Massé, Numerical Modeling of magnetic Field Flow Fractionation in Microchannels: a two-fold approach using particle trajectories and concentration, *Proceedings of MSM Conference*, 2001, pp. 202–205.
- 25 University of Minnesota, Supercomputing Institute, Flow and Transport in porous Media, *Newsletter*, 1999, vol. 16, no. 1.
- 26 G. Goranovic, I. Perch-Nielsen, U. Larsen, A. Wolff, J. Kutter and P. Tellman, Three-dimensional single step flow sheathing in micro cell sorter, *Proceedings of MSM Conference*, 2001, pp. 242–245.
- 27 L. Lee, M. Madou, K. Koelling, S. Daunert, S. Lai, C. Koh, Y. Juang, Y. Lu and L. Yu, Design and Fabrication of CD-like microfluidic Platforms for Diagnostics: polymer-based Microfabrication, *Biomedical Microdevices*, 2001, 3:4, 339–351.
- 28 P. Senkars, V. de Biasi and D. Barrow, Computational Simulations of Fluid Flow Dynamics, and Bead Packing in solid Phase Extraction Microsystems, *Proceedings of  $\mu$ TAS Conference*, ed. Y. Baba, S. Shoji and A. van den Berg, 2002, vol. 1, pp. 76–78.
- 29 Z. Guo and T. S. Zhao, Lattice Boltzmann Model for incompressible Flows through porous Media, *Phys. Rev. E*, 2002, 66, 036304.